Engineering Fracture Mechanics 79 (2012) 213–224

Contents lists available at SciVerse ScienceDirect

Engineering Fracture Mechanics

journal homepage: www.elsevier.com/locate/engfracmech

Fracture behaviour of linear low density polyethylene – fumed silica nanocomposites

Andrea Dorigato *, Alessandro Pegoretti

Department of Materials Engineering and Industrial Technologies and INSTM Research Unit, University of Trento, via Mesiano 77, 38123 Trento, Italy

ARTICLE INFO

Article history:
Received 1 August 2011
Received in revised form 20 October 2011
Accepted 30 October 2011

Keywords:
Polyethylene
Fumed silica
Nanocomposites
Essential work of fracture

ABSTRACT

The role of fumed silica nanoparticles, having different surface area and surface treatments, on the fracture behaviour of a linear low density polyethylene (LLDPE) matrix was investigated. Tensile tests under quasi-static and impact conditions evidenced beneficial effects on both the elastic modulus and the strain at yield. By the essential work of fracture approach, increments of both the initiation and the propagation components of the specific essential work of fracture terms were highlighted. Dilatometric measurements excluded the filler–matrix debonding as a possible toughening mechanism, while a progressive alignment of silica aggregates was detected by TEM observations.

1. Introduction

In the last decades, it has been widely proven that the addition of inorganic nanofillers to polymeric matrices may lead beneficial effects, such as higher dimensional stability [1,2], moisture and gas barrier [3,4], enhanced mechanical properties [5–8], and improved flame retardancy [9]. From the first industrial application of nylon–clay nanocomposites 25 years ago [10], many efforts were devoted to the development of nanocomposite materials by using various polymeric matrices and nanofillers [11]. Nanocomposites were successfully prepared by using rather hydrophilic polymers, such as polyamides or polyurethanes. In fact, the extremely high aspect ratio of nanostructured inorganic materials can be exploited when the filler is homogeneously dispersed in the polymeric phase. On the other hand, the relatively low dispersion quality of inorganic nanofillers in polyolefins is one of the main problems to overcome [5,12].

Due to its combination of low cost, high chemical resistance and relatively good mechanical properties, polyethylene is the most widely used polyolefin [12,13]. In particular, linear low-density polyethylene (LLDPE) finds wide application in film production for the packaging industry, because of its high tear and impact strength. LLDPE is a copolymer of ethylene and an α-olefin or diene, such as butene, hexene or octene [5]. As a consequence, LLDPE is formed by a linear hydrocarbon backbone with short chain branching. It has been reported that the addition of various nanofillers to LLDPE may lead to an increase of the elastic modulus and in some cases of its tensile strength. However, these improvements are often accompanied by a certain embrittlement, with a strong reduction of the elongation at break. Among various nanofillers proposed to reinforce LLDPE, organo-modified clays were surely the most studied [14,15], while less attention was devoted to inorganic nanoparticles such as silica, titania, and zirconia. Chaichana et al. [16] developed a new technique to synthesize LLDPE/nanosilica systems via in situ polymerization with a zirconocene/MAO catalyst, in order to study the effect of particle size on the catalytic properties of the resulting materials. Jongsomjit et al. [17] investigated the effect of SiO_2 and ZrO_2 nanoparticles on the microstructure of LLDPE nanocomposites synthesized via in situ polymerization with zirconocene. Wang studied the

* Corresponding author. Tel.: +39 0461 882412; fax: +39 0461 881977.
E-mail address: andrea.dorigato@ing.unitn.it (A. Dorigato).

0013-7944/$ - see front matter © 2011 Elsevier Ltd. All rights reserved.
doi:10.1016/j.engfracmech.2011.10.014

Nomenclature

B	specimen thickness
DENT	double edge notched tension
E	tensile modulus
EWF	essential work of fracture
H	distance between the grips
L	ligament length
$\bar{L}$	arithmetic mean of the ligament length
LLDPE	linear low density polyethylene
n	number of specimens
MAO	methyl-alumoxane
R^2	coefficient of determination
S	standard error of the linear regression
$\bar{S}$	standard deviation of W_f values from the least squares fitted line
S_{11}, S_{12}, S_{22}	parameters of the linear regression
TEBqs	specific tensile energy to break under quasi-static conditions
TEBi	specific tensile energy to break under impact conditions
TEM	transmission electron microscopy
V_0	volume in the undeformed state
W	specimen's width
W_e	work expended in the fracture process zone
W_{ini}	total work of fracture initiation
W_f	total work of fracture
$\overline{W_F}$	arithmetic mean of W_f values
W_{LLDPE}	weight fraction of LLDPE in the composites
W_p	work associated to the plastic deformation outside the fracture zone
w_e	specific essential work of fracture
w_f	specific total work of fracture
w_{ini}	specific essential work of crack initiation
w_p	specific non-essential work of fracture
X_c	crystallinity degree
β	shape factor for the outer plastic zone
ΔV	volume variation
ΔH_m	melting enthalpy
ε_b	strain at break
ε_y	strain at yield
ε_1	axial strain
ε_2	transversal strain
σ_b	stress at break
$\sigma_{\max}$(mean)	mean maximum stress
σ_y	stress at yield

dispersion behaviour of TiO_2 nanoparticles in LLDPE/LDPE/TiO_2 nanocomposites [18]. To our knowledge, only Kontou and Niaounakis [5] analyzed the thermo-mechanical properties of LLDPE – fumed silica nanocomposites, obtaining significant improvements both of the stiffness and the tensile properties at break.

From a general point of view, the fracture behaviour of polymer nanocomposites is mainly governed by the dispersion degree of the nanofiller and from the polymer–filler interfacial interaction [14,19]. The presence of a proper functionalization on the surface of the nanoparticles may lower the filler–filler interaction and promote their fine dispersion in the matrix. Moreover, it could lead to a more efficient stress transfer mechanism at the interface. Some controversial results are reported in the scientific literature on the effect of surface functionalization of nanofillers [20,21]. Also the role of void formation during the deformational process of the material is still debated in literature [22]. In the most cases, interface-initiated cavitation, followed by void growth and coalescence, seems to be the major factor responsible for the enhancement of fracture toughness exhibited by particulate nanocomposites [23]. The orientation of the filler along the strain direction could play an important role on the fracture toughness of the material, and also the changes in the crystalline morphology of the matrix (i.e. the size and form of crystals) may often influence the failure properties of semi-crystalline polymer matrices [24].

In recent years, the effectiveness of fumed silica nanoparticles in improving the mechanical properties and the thermal stability of various polyolefins has been investigated by our group [25–28]. In the present paper, we focused our attention on the effect of various kinds of fumed silica nanoparticles, different for their size and for the presence of the organomodification, on the mechanical properties of LLDPE based nanocomposites, prepared through a melt compounding process. A particular attention has been devoted to their fracture behaviour evaluated by the essential work of fracture (EWF) approach.

2. Experimental

2.1. Materials and preparation of the samples

A series of Aerosil® commercial fumed silica were kindly supplied by Degussa (Hanau, Germany), with different surface area (ranging from 90 $m^2\ g^{-1}$ for the Aerosil 90 up to 380 $m^2\ g^{-1}$ for the Aerosil 380) and surface treatment. In particular Aerosil r816 is obtained by functionalizing Aerosil 200 with hexadecylsilane. Flexirene® CL10 linear low density polyethylene (density = 0.917 g cm^{-3}, MFI at 190 °C and 2.16 kg = 2.6 g $(10\ min)^{-1}$), kindly supplied by Polimeri Europa (Mantova, Italy), was selected as polymer matrix.

Silica nanoparticles were melt compounded with LLDPE in a Thermo Haake® internal mixer (Karlsruhe, Germany) at 170 °C for 15 min and 90 rpm. Fumed silica was slowly added in the hot chamber of the mixer, immediately after the complete melting of the LLDPE. The compounded materials were then hot pressed in square sheets about 0.8 mm thick by using a Carver® Laboratory press (Wabash, IN, USA) operating at 170 °C and 0.2 kPa. For all samples the filler content was fixed at 2 vol.%. ISO 527 type 1BA specimens were punch-cut from the sheets. LLDPE indicates the unfilled material, while the nanocomposites were designated by the type of matrix, followed by the filler type (for example LLDPE-A90 indicates the nanocomposite filled with 2 vol.% of Aerosil 90).

2.2. Testing procedures

Uniaxial tensile tests were performed with an Instron 4502 electromechanical testing machine (Norwood, MA, USA) on ISO 527 type 1BA specimens. According to ISO 527 standard, elastic modulus was evaluated as secant modulus between deformation levels of 0.05% and 0.25%. In order to acquire a sufficient amount of data, a limited testing speed (0.25 mm min^{-1}) was utilized for these tests. The strain was monitored through a resistance extensometer Instron® model 2620-601 (gage length = 12.5 mm). Tensile test at break were carried out at a crosshead speed of 50 mm min^{-1} without using the extensometer. Instrumented tensile tests under impact conditions were performed by using a CEAST® Resil Impactor (Turin, Italy). The hammer impacted the specimens at a speed of 2 m s^{-1} with an energy of 7.3 J.

Being LLDPE a highly ductile polymer mostly used for thin products, such as films or sheets, an elasto-plastic fracture mechanics approach was selected to characterize the material fracture toughness under plane-stress conditions. In particular, the essential work of fracture (EWF) concept has been adopted. The EWF method has gained an extended popularity for the evaluation of the fracture toughness of highly ductile polymers [29,30]. A review on the application of the essential work of fracture (EWF) concept for polymers and composite materials has been recently authored by Barany et al. [31]. This method is based on the hypothesis that the total work of fracture W_f of a notched specimen is the summation of two contributes: the work expended in the fracture process zone, W_e, which is considered to be essential for creating new fracture surfaces, and the work associated to the plastic deformation outside the fracture zone, W_p [23,32]. In Fig. 1, the fracture process zone in a double edge notched (DENT) sample is depicted, while in Fig. 2 a representative load–displacement curve is reported. Under plane-stress conditions, W_e is proportional to the ligament cross-section, LB, and W_p is proportional to the outer plastic volume βL^2 as follows:

$$W_f = LBw_f = LBw_e + \beta L^2 Bw_p \tag{1}$$

therefore,

$$w_f = w_e + \beta w_p L \tag{2}$$

where B is the specimen thickness, β is a shape factor for the outer plastic zone, and w_f, w_e, w_p are the specific total, essential, and non-essential work of fracture terms.

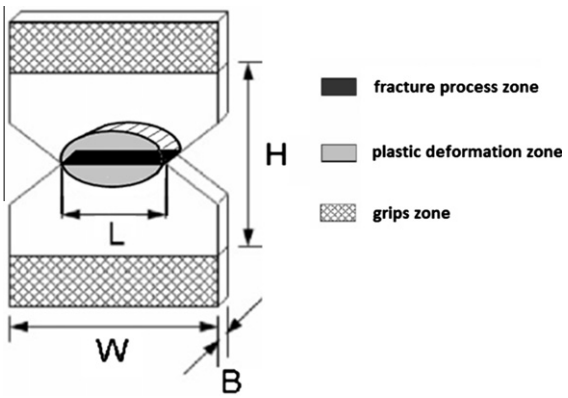

Fig. 1. Schematic of DENT samples for EWF test.

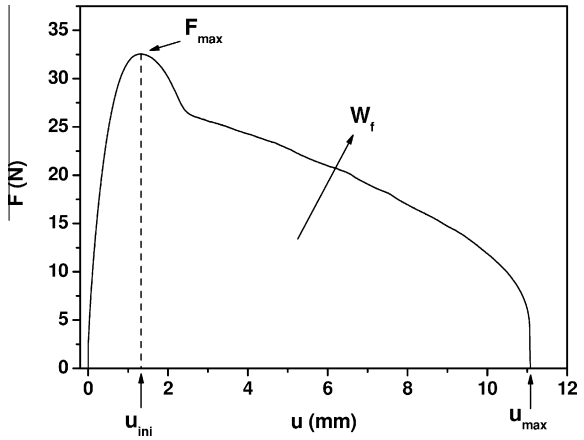

Fig. 2. Representative curves of a tensile test on a DENT specimens of neat LLDPE.

Specimens dimensions were chosen according to the indications reported in the paper of Williams and Rink about the standardisation of the EWF test [30]. Generally the samples should be less than 1 mm thick, while ligament length should be comprised in a interval between 5 mm and 15 mm. Specimens' width and height should be at least 30 mm. In order to obtain standard deviation values over mean value of w_e of <0.1, at least 20 specimens should be tested. According to these indications, specimen's dimensions were selected as follows: $W = 30$ mm, $H = 30$ mm, total height = 50 mm, $B = 0.8$ mm, 5 mm < L < 13 mm. EWF tests were conducted at a crosshead speed of 10 mm min^{-1}, and at least 20 specimens were tested for each sample. To obtain a sharp crack tip (crack tip radius <2 μm), notches were prepared by using a razor blade.

In order to check the validity of the experimental data, the maximum stress on the ligament should be compared to the tensile yield stress (σ_y). Considering that the ligament is constrained laterally, this value would be expected to be $1.15\sigma_y$ [31]. The results are assumed to be valid if the stress is within the range of $0.9–1.1\sigma_{max}$(mean). The w_f versus L data are then subjected to a linear regression, and the following parameters should be determined:

$$S_{11} = \Sigma(w_{fi} - \overline{w_f})^2 \tag{3a}$$

$$S_{22} = \Sigma(L_i - \overline{L})^2 \tag{3b}$$

$$S_{12} = \Sigma(w_{fi} - \overline{w_f})(L_i - \overline{L}) \tag{3c}$$

$$n\overline{L} = \Sigma Li \tag{3d}$$

$$n\overline{w_f} = \Sigma w_f i \tag{3e}$$

where the summation is taken over $i = 1 - n$, being n the number of observations. Thus:

$$w_e = \overline{w_f} - \overline{L}\left(\frac{S_{12}}{S_{22}}\right) \tag{3f}$$

$$\beta w_p = \left(\frac{S_{12}}{S_{22}}\right) \tag{3g}$$

and the standard error S of w_e is:

$$S^2 = \left(\frac{1}{n} + \frac{\overline{L^2}}{S_{22}}\right)\frac{1}{(n-2)}\left(S_{11} - \frac{\overline{S_{12}^2}}{S_{22}}\right) \tag{3h}$$

$$R^2 = \left(\frac{S_{12}^2}{S_{11}\cdot S_{22}}\right) \tag{3i}$$

Any data point laying outside the interval of $\pm 2\overline{S}$, where $\overline{S}$ is the standard deviation of the w_f values from the least squares fitted line, is excluded and the line recalculated. $\overline{S}$ can be computed with the following expression:

$$\overline{S}^2 = \frac{1}{n-2}\left(S_{11} - \frac{S_{12}^2}{S_{22}}\right) \tag{3j}$$

These exclusion criteria were systematically utilized to assess the quality of the data in our analysis. As reported in some papers [33,34], it is also possible to evaluate the total work of fracture initiation (W_{ini}) through an integration of load–displacement curves until the maximum load is reached. W_{ini} is proportional to the ligament cross-section, LB, and the specific essential work of crack initiation (w_{ini}) can be therefore determined though the linear regression of specific work of fracture initiation versus L data.

In order to detect the occurrence of filler–matrix debonding phenomena and/or void formation during the application of the load, dilatometric tests were carried out on neat LLDPE and LLDPE-A380 samples. Rectangular specimens 100 mm long, 10 mm wide and 4 mm thick, prepared by melt compounding and subsequent hot pressing, were tested. Specimens were deformed intension with the Instron® machine at a crosshead speed of 5 mm min^{-1}. At least three specimens were tested for each sample at room temperature. During the tests, both longitudinal and transversal deformations were simultaneously monitored by using an Instron® 2620 bi-axial extensometer. Considering that for a transversely isotropic material the two lateral strain components are equal, the volume strain is then given by:

$$\frac{\Delta V}{V_0} = (1+\varepsilon_1)\cdot(1+\varepsilon_2)^2 - 1 \tag{4}$$

where ΔV is the volume variation, V_0 the volume in the undeformed state, ε_1 the axial strain, and ε_2 the transversal strain. Volume strain is measured assuming that the changes in the thickness and width are the same, that the sample cross section remains rectangular and the deformation is affine (non-necking in the measured zone). For both neat LLDPE and filled specimens the deformation started to be non homogeneous throughout the specimen for the presence of a necked zone at elongation levels of about 30%. Therefore, the volume variation was evaluated up to a strain level of 10%. No evidence of differential changes in width and thickness were noticed within this deformation level, and the cross section maintained a rectangular shape.

In order to investigate the influence of silica nanoparticles on the crystallization behaviour of LLDPE and its composites, differential calorimetric analysis was carried out. A Mettler DSC30 differential scanning calorimeter (Schwerzenbach, Switzerland) was used to test the samples utilized for dilatometric tests. All the measurements were performed under a nitrogen flow of 100 ml min^{-1}. The specimens were first heated at a rate of 10 °C min^{-1} from 0 °C to 200 °C, and then cooled to room temperature at a cooling rate of 10 °C min^{-1}. A second heating stage was performed at the same heating rate until 200 °C. The melting enthalpy (ΔH_m) was determined by integrating the specific power peaks in the heating thermograms, and the crystallinity degree (X_c) of LLDPE in the composites was calculated in the first heating stage as follows:

$$X_c = \frac{\Delta H}{\Delta H_0 \cdot W_{LLDPE}} \cdot 100 \tag{5}$$

where ΔH is the apparent enthalpy of fusion per unit mass of composite, ΔH_0 is the heat of fusion of fully crystalline polyethylene, taken as 290 J g^{-1} [35], and W_{LLDPE} is the weight fraction of LLDPE in the composites.

Transmission electron microscopy (TEM) observations were performed in order to evaluate the dispersion of silica aggregates in both undeformed and deformed specimens. A Philips®/FEI CM120 TEM (Hillsboro, Oregon, USA) was utilized, at an acceleration voltage of 80 kV. Thin sections of LLDPE-A380 nanocomposite were sliced at a temperature of −70 °C by using a Reichert–Jung Ultracut FC4E crio-ultramicrotome (Depew, NY, USA). TEM observations were carried out on specimen tested in quasi-static tensile conditions at various longitudinal strain levels (0%, 30%, 60%, 100%).

3. Results and discussion

3.1. Uniaxial tensile tests on un-notched samples

Representative stress–strain curves of quasi-static tensile tests at break on neat LLDPE and relative nanocomposites are reported in Fig. 3, while the main parameters derived from the curves are summarized in Table 1. It can be noticed that the introduction of 2 vol.% of untreated fumed silica nanoparticles in the LLDPE matrix leads to a remarkable increase of the elastic modulus. For instance, LLDPE-A300 sample shows an enhancement of the material stiffness of more than 50% with respect to the neat matrix. The stiffness of LLDPE-Ar816 sample is practically the same of specimens filled with hydrophilic fumed silica with the same surface area (A200). Considering the standard deviation values, neither particle size nor the presence of a surface treatment seem to play a clear effect on the stiffness of the samples. This is not surprising, since earlier studies on both particulate and fibre reinforced composites proved that interfacial adhesion and structure influence stiffness to a much lower extent with respect to ultimate properties (such as tensile yield stress or tensile strength) [36,37]. The stress at yield (σ_y) slightly increases with the surface area of the nanofiller, and this improvement is more evident when functionalized silica nanoparticles are used. The same conclusions can be drawn for the stress at break (σ_b) and the strain at break (ε_b) values. Consequently, specific tensile energy to break under quasi-static conditions (TEBqs) values, obtained by integrating the stress–strain curves are remarkably increased by nanosilica addition, especially when surface treated nanoparticles are involved. In fact, neat LLDPE sample shows a TEBqs value of 191.3 MJ m^{-3}, while for LLDPE-Ar816 composite a TEBqs value of 283.3 MJ m^{-3} is measured.

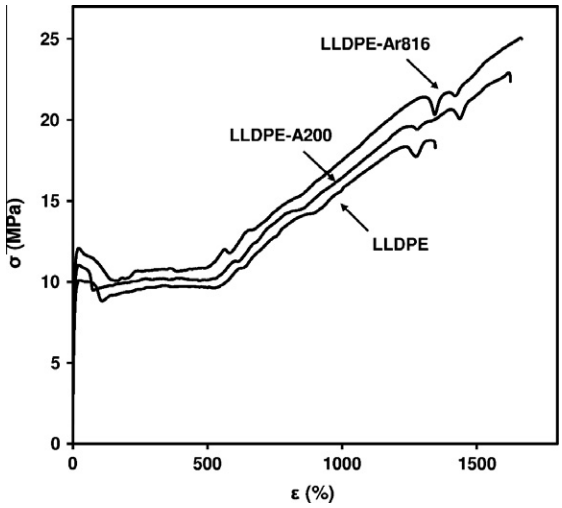

Fig. 3. Representative curves of quasi-static tensile tests at break on neat LLDPE and relative nanocomposites.

Table 1
Tensile modulus (E), yield stress (σ_y), yield strain (ε_y) stress at break (σ_b), strain at break (ε_b) and tensile energy to break (TEBqs) under quasi-static conditions for neat LLDPE and relative nanocomposites.

	E (MPa)	σ_y (MPa)	ε_y (%)	σ_b (MPa)	ε_b (%)	TEBqs (MJ m^{-3})
LLDPE	199 ± 27	10.1 ± 0.1	26.6 ± 0.1	19.8 ± 2.0	1439 ± 141	191.3 ± 30.6
LLDPE-A90	262 ± 25	10.8 ± 0.1	24.8 ± 0.2	22.6 ± 0.3	1625 ± 49	232.3 ± 6.0
LLDPE-A200	274 ± 6	11.0 ± 0.1	24.1 ± 1.3	22.3 ± 0.9	1613 ± 78	236.0 ± 17.3
LLDPE-A300	311 ± 41	11.1 ± 0.1	22.9 ± 0.6	22.9 ± 1.1	1637 ± 76	242.7 ± 18.0
LLDPE-A380	285 ± 46	11.1 ± 0.1	23.9 ± 0.5	23.3 ± 0.3	1722 ± 40	257.0 ± 9.0
LLDPE-Ar816	275 ± 10	12.0 ± 0.1	22.8 ± 0.5	25.7 ± 0.7	1738 ± 65	283.3 ± 16.0

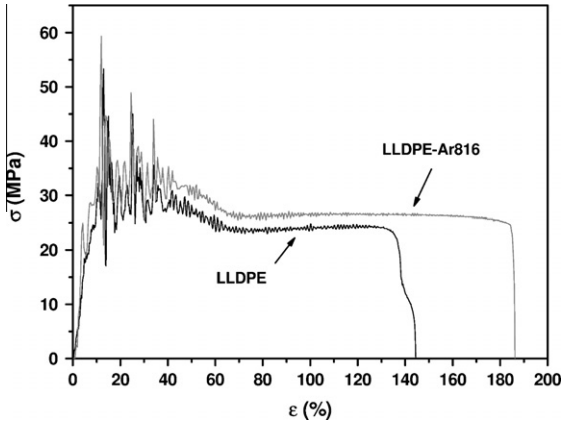

Fig. 4. Representative curves of tensile impact tests on neat LLDPE and LDPE-Ar816 nanocomposite.

The toughening effect provided by silica nanoparticles on the LLDPE matrix can be evidenced also under tensile impact conditions. An example of the stress–strain curves typically obtained from tensile impact test are reported in Fig. 4, while specific tensile energy to break under impact conditions (TEBi) values of all the tested samples are compared in Fig. 5. Specific tensile energy adsorbed under impact conditions is positively affected by the introduction of fumed silica nanoparticles. A slight increase of TEBi values can be detected when hydrophilic nanoparticles are utilized, while the enhancement is more evident when functionalized nanoparticles are used. In fact, for neat LLDPE an impact TEBi value of 20.6 MJ m^{-3}, can be measured, while for LLDPE-Ar816 nanocomposite a higher TEBi value of 28.7 MJ m^{-3} is reached. Referring to the experimental

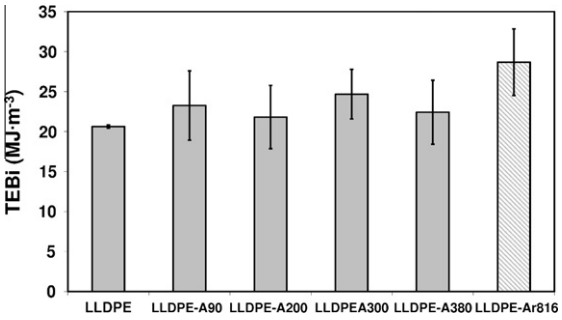

Fig. 5. Tensile energy to break under impact conditions (TEBi) values for LLDPE and relative nanocomposites.

curves reported in Fig. 4, it could be interesting to observe the presence of an evident stress oscillation after the yield stress is reached. A similar behaviour was reported by Karger-Kocsis et al. on semicrystalline polymers (i.e. PET, copolyesters) tested under tensile impact conditions [38,39]. In those papers, no striation bands and no crystallization could be detected after yield, and an adiabatic shear banding seemed to be the dominant deformation mode. Furthermore, the occurrence of stress oscillation was limited to a given impact speed or frequency range. However, the polymer tested in the present paper (LLDPE) has a very different chemical structure and crystalline properties with respect to the copolyesters studied by Karger-Kocsis. Moreover, in this work tensile impact tests were performed only at a fixed testing configuration (i.e. testing speed, specimens' thickness etc.). Therefore, it is very difficult to assess whether the observed stress oscillations are due to the sample deformation mode, or to inertial effects of the measuring device.

In order to have a better comprehension of the results coming from tensile tests, the role played by the dispersed nanofiller and by the filler–matrix interaction should be taken into account. For as concerns (untreated) hydrophilic fumed silica nanoparticles, the extent of polymer–filler interaction depends on the contact area available at the interface. An increase in the nanofiller surface area generally leads to an enhancement of the interfacial interaction and to a more efficient stress-transfer mechanism at the interface. As suggested by Zhang et al. [40], it is possible that the presence of a surface treatment decreases the surface energy of the nanoparticles, thus inducing a reduction of the intensity of particle–particle interactions and a finer dispersion in the matrix. Furthermore, in many cases filler–matrix interaction is reported to decrease when nanofiller are surface treated [21]. In fact, in a previous work on high density polyethylene – fumed silica nanocomposites, we found that the surface treatment considerably improved the nanofiller dispersion within the matrix [41]. Therefore, from quasi-static and impact tensile tests on un-notched samples, it can be concluded that (i) untreated nanoparticles at higher surface area (A380) are more effective in increasing elastic modulus because of the higher extent of the surface interaction; (ii) silica functionalization significantly contributes to the improvement of the tensile properties at break, probably because of a finer dispersion of nanofiller aggregates within the matrix.

3.2. Essential work of fracture evaluation

EWF tests have been performed with the aim to confirm and shed some light on the toughening effect provided by the silica nanoparticles in the LLDPE matrix. Fig. 6 reports plots of specific work of fracture (w_f) versus ligament length of neat LLDPE and of the relative nanocomposites, while the most important parameters derived from the EWF tests are collected in Table 2. In accordance with quasi-static tensile tests on un-notched specimens, it is proven that the introduction of silica nanoparticles actually leads to remarkable improvements of the essential work of fracture (w_e) parameter. In particular, the highest w_e value is determined for LLDPE-A380 nanocomposite, with an enhancement of the 43% over neat LLDPE matrix. Interestingly, the increase of essential work of fracture with the surface area of the nanofiller is accompanied by a progressive reduction of the specific non-essential term (βw_p) related to the plastic work dissipated in the non-process zone. According to the existing literature [22], the observed reduction of the βw_p term can be attributed to a restriction of the ductile deformation caused by physical constraint due to polymer–filler interaction. Also the essential work of crack initiation is positively affected by the introduction of fumed silica nanoparticles. In fact, w_{ini} values increase with the nanofiller surface area. On the other hand, this energy repartition puts in clear evidence that the major part of the observed enhancement in fracture toughness is related to the crack propagation component. w_e values for nanocomposites filled with functionalized silica are practically the same of those obtained for nanocomposites based on untreated silica nanoparticles with the same surface area (i.e. around 31 kJ m^{-2}), while the non-essential term is practically equal to that of the neat matrix. As mentioned before, surface treatment of silica nanoparticles improves the dispersion of the aggregates within the matrix but decreases polymer–filler interaction. In these conditions, matrix shear yielding and energy absorption through plastic deformation are thus favoured. This means that the effect of the better filler dispersion due to functionalization is partially counterbalanced by the reduction of the filler matrix-interaction. In all the investigated cases, R^2 value is around 0.99, thus indicating a satisfactory linearity of the data with a reduced dispersion. This is one of the requisite for the applicability of the method as indicated by Williams and Rink in their notes on the standardisation of the EWF method [30].

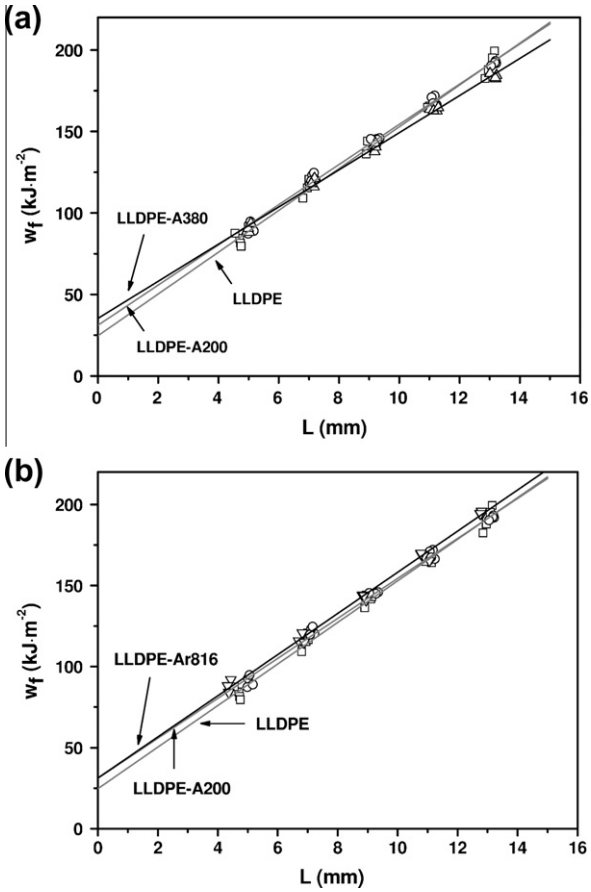

Fig. 6. Plots of specific work of fracture (w_f) versus ligament length of neat LLDPE and relative nanocomposites. (a) Effect of the nanofiller surface area and (b) effect of the surface functionalization. (□) LLDPE, (○) LLDPE-A200, (△) LLDPE-A380, (▽) LLDPE-Ar816.

Table 2
EWF parameters for neat LLDPE and relative nanocomposites.

	w_e (kJ m^{-2})	βw_p (MJ m^{-3})	R^2	w_{ini} (kJ m^{-2})	R^2
LLDPE	24.7 ± 2.7	12.8 ± 0.3	0.991	2.3 ± 0.3	0.994
LLDPE-A90	21.0 ± 2.7	13.1 ± 0.3	0.991	2.4 ± 0.5	0.987
LLDPE-A200	31.1 ± 2.2	12.3 ± 0.2	0.994	3.6 ± 0.4	0.987
LLDPE-A300	28.4 ± 2.3	12.2 ± 0.2	0.993	3.2 ± 0.4	0.988
LLDPE-A380	35.3 ± 1.8	11.4 ± 0.2	0.995	3.5 ± 0.3	0.995
LLDPE-Ar816	31.2 ± 2.1	12.7 ± 0.2	0.995	3.3 ± 0.6	0.982

The errors indicated in the table are standard errors of linear fit.

3.3. Volume strain measurements

Lazzeri et al. [42] analyzed the debonding mechanism during tensile tests in HDPE/calcium carbonate nanocomposites, and reported that stress whitening zones appeared inside the gauge length region during tensile tests. This phenomenon was attributed to the matrix-particle debonding and the consequent void growth. The concurrent increase of the volume strain with axial deformation confirmed their hypothesis. Moreover, TEM observations showed cavities and voids due to debonding and deformation bands in the stress whitened areas. Also Sudar et al. conducted volume strain measurements on LDPE/$CaCO_3$ nanocomposites, by using various filler amounts [43]. Considering that in thermoplastic matrices filler–matrix debonding and plastic deformation of the matrix through shear yielding are competitive processes, they found that the number of voids formed during the deformational process was inversely proportional to the stiffness of the matrix. In stiff matrices (i.e. elastic modulus higher than 1 GPa) almost the entire amount of filler separated from the matrix under the effect of external load, while for soft matrices (with an elastic modulus lower than 0.4 GPa) the debonding was completely absent and the composite could deform exclusively by shear yielding.

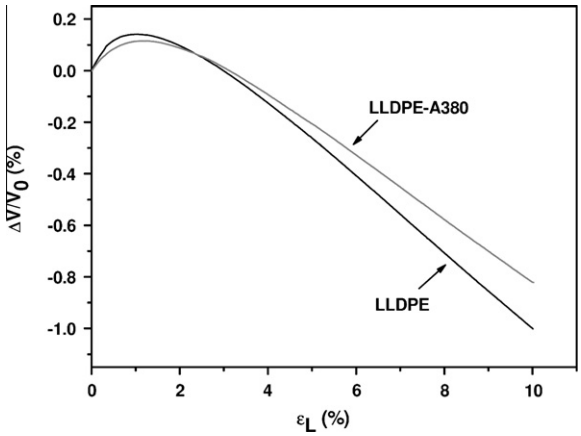

Fig. 7. Volume strain versus axial strain for neat LLDPE and LLDPE-A380 nanocomposites.

Table 3
DSC results for neat LLDPE and relative nanocomposites.

	Undeformed specimens			Specimens deformed at $\varepsilon = 100\%$		
	T_m (°C)	ΔH_m (J g^{-1})	X_c (%)	T_m (°C)	ΔH_m (J g^{-1})	X_c (%)
LLDPE	123.0	120.8	41.7	122.0	113.3	39.1
LLDPE-A90	123.6	122.2	42.1	121.7	114.7	39.5
LLDPE-A200	123.0	123.3	42.5	121.4	115.5	39.8
LLDPE-A300	123.1	124.8	43.0	121.6	109.5	37.8
LLDPE-A380	123.0	123.1	42.4	121.4	113.3	39.1
LLDPE-Ar816	123.7	119.4	41.2	121.6	115.8	39.9

Samples were taken from dilatometric tests.

Taking these results into account, dilatometric measurements were thus performed, in order to characterize the deformational behaviour of the samples at various strain levels. In Fig. 7, the relative volume strain versus the longitudinal strain is plotted for the neat matrix and for the LLDPE-A380 nanocomposite, respectively. Moreover, in Table 3 the results of the DSC analysis performed on the same samples before ($\varepsilon = 0\%$) and after the yielding ($\varepsilon = 100\%$) are summarized. A progressive decrease of the volume strain with the deformation can be detected for the neat LLDPE. Lazzeri, following the considerations of Gaucher-Miri et al. [44], suggested that this decrease could be probably attributed to the stretching of the amorphous segments along the strain direction, leading to the formation of a mesomorphic structure and to a decrease of the volume strain [42]. The decrease in volume strain observed for neat LLDPE cannot be attributed to further crystallization, being the crystallinity of yielded samples slightly reduced with respect of unloaded ones (Table 3).

More generally, the addition of silica nanoparticles seems to have a very limited influence on the crystalline properties of the LLDPE. It could be important to underline that crystalline behaviour of the samples was evaluated also by X-ray diffraction tests (not reported in the paper for the sake of brevity). Referring the Whole Powder Pattern Model (WPPM) [45,46], it was demonstrated how the mean size of the LLDPE crystallites was unaffected by the presence of the nanoparticles. As reported in our previous papers on LLDPE nanocomposites systems [26,28,41,47], this behaviour could be tentatively explained considering the amorphous nature of silica nanofillers. However, a deeper investigation is required to assess the contribution of amorphous nanoparticles on the crystallization behaviour of the investigated materials.

But the most important result is that the volume strain decreases with the deformation for the LLDPE-A380 composite too. Considering that the elastic modulus of neat LLDPE is about 0.2 GPa, this experimental evidence is in contrast with the observations of Lazzeri et al. [42] and in accordance with the conclusions reported by Sudar et al. [43]. This probably means that in our system the filler–matrix debonding mechanism is absent and the composite deforms by shear yielding.

3.4. Transmission electron microscopy observations

More information about the toughening mechanism provided by silica nanoparticles at higher strains can be obtained from TEM images of LLDPE-A380 composite at various deformation levels, reported in Fig. 8a–d. First of all, it can be noticed that the nanofiller is dispersed in the matrix in aggregates with a diameter of about 300–400 nm. However, it is difficult to assess if these clusters are constituted by aggregates of primary nanoparticles formed during the manufacturing process or constituted by physical agglomeration of aggregates. The aggregates remain iso-dimensional up to an applied strain of 30%, while for higher deformation levels a pronounced orientation along the stress direction is evident. This means that after the

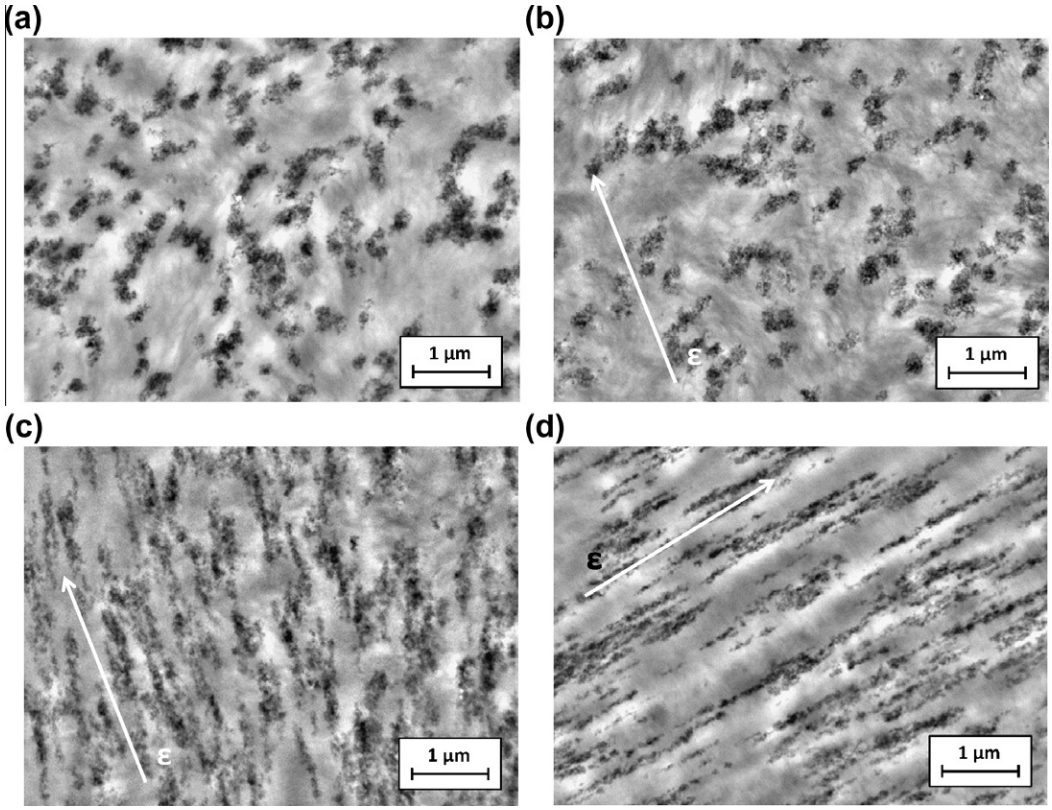

Fig. 8. TEM images of LLDPE-A380 nanocomposite tested at various axial strain levels: (a) 0%, (b) 30%, (c) 60%, and (d) 100%.

strain at yield (ε_y), the shear yielding process becomes very intense and the nanoparticles align along the strain direction. For a strain of 100%, silica aggregates are about 2 μm long and less than 100 nm large, and distanced by about 100 nm. Considering that DSC tests did not evidence any influence of the nanoparticles on the crystalline properties of the matrix, it is possible to hypothesize that during the viscous flow produced by shear yielding the nanoparticles are segregated in the amorphous regions separated by highly oriented crystalline domains. This experimental evidence is supported by the observations of Jeol et al. [48], who analyzed the deformation-induced modification of the dispersion state of silica nanoparticles in poly(ethyleneterephtalate) nanocomposites, after a stretch-blowing process just above the glass transition temperature of the material. In that work fumed silica nanoparticles were shown to agglomerate and orient parallel to the elongation direction, forming long streams of aggregates (more than 2 μm) regularly spaced by a distance of 50–100 nm. They concluded that the nanoparticles were rejected from the highly oriented crystalline domains induced by the strain, on the contrary of what happened using spherical silica nanoparticles, for which the long streams of nanoparticles where oriented perpendicular to the elongation direction. They hypothesized that this unexpected orientation was produced by the extended growth of mesophases and crystallites perpendicular to the orientation, forming stacked lamellae rather than microfibrils. Also TEM images reported in the present paper excluded void formation due to interfacial debonding as a possible toughening mechanism for these nanocomposites at all the investigated strain, probably for the relatively high filler–matrix interaction. Unfortunately, we could not observe composites filled with functionalized nanoparticles, for whose the lowering of filler–matrix interaction might favour local debonding at the interface. Further investigations are needed to reach a deeper comprehension of the deformational behaviour at elevated strain. It could be hypothesized that the long streams of aggregates along the stress direction may favour load transfer mechanism at the interphase and supplementary energy consumption for their alignment along the strain direction. In these conditions the load sustained by the polymeric phase is reduced and LLDPE macromolecules can deform at a higher extent before breaking. Moreover, silica aggregates could also play the role of a solid state lubricant, thus favouring the deformation along the strain direction.

4. Conclusions

Various kinds of fumed silica nanoparticles, differing for their size and for surface treatment, were melt compounded with a linear low density polyethylene matrix, in order to investigate their effect on the fracture behaviour of the resulting materials. A significant increase of the elastic modulus and elongation at break due to nanofiller introduction was observed both under quasi static and impact conditions, especially when functionalized nanoparticles were utilized.

The application of the essential work of fracture approach confirmed the increase of the plane stress fracture toughness due to nanosilica addition, being w_e values positively affected by the presence of high surface area untreated nanoparticles. Dilatometric tests excluded the presence of filler–matrix debonding mechanisms during the deformational process, while TEM images indicated the occurrence of a strong alignment of silica aggregates along the strain direction for elevated deformations. These microstructural features seemed to be responsible of the toughening effect due to the presence of silica nanoparticles in the material.

Acknowledgment

The authors are grateful to Polimeri Europa® S.p.A for the kind provision of LLDPE chips and for TEM observation for this work. This research activity has been performed in the Framework of the scientific and Technological co-operation Agreement between Italy and Hungary for the years 2011–2013.

References

[1] Bondioli F, Dorigato A, Fabbri P, Messori M, Pegoretti A. High-density polyethylene reinforced with submicron titania particles. Polym Engng Sci 2008;48:448–57.
[2] Bondioli F, Dorigato A, Fabbri P, Messori M, Pegoretti A. Improving the creep stability of high-density polyethylene with acicular titania nanoparticles. J Appl Polym Sci 2009;112:1045–55.
[3] Grunlan JC, Grigorian A, Hamilton CB, Mehrabi AR. Effect of clay concentration on the oxygen permeability and optical properties of a modified poly(vinyl alcohol). J Appl Polym Sci 2004;93:1102–9.
[4] Kim JK, Hu C, Woo RSC, Sham ML. Moisture barrier characteristics of organoclay–epoxy nanocomposites. Compos. Sci. Technol. 2005;65:805–13.
[5] Kontou E, Niaounakis M. Thermo-mechanical properties of LLDPE/SiO_2 nanocomposites. Polymer 2006;47:1267–80.
[6] Pegoretti A, Dorigato A, Penati A. Tensile mechanical response of polyethylene – clay nanocomposites. Express Polym Lett 2007;1:123–31.
[7] Pegoretti A, Dorigato A, Penati A. Contact angle measurements as a tool to investigate the filler–matrix interactions in polyurethane–clay nanocomposites from blocked prepolymer. Eur Polym. J 2008;44:1662–72.
[8] Pegoretti A. Editorial corner – a personal view. Nanocomposite fibres: a strategy for stronger materials? Express Polym Lett 2010;4:669.
[9] Zhang J, Jiang DD, Wilkie CA. Fire properties of styrenic polymer–clay nanocomposites based on oligomerically-modified clay. Polym Degrad Stab 2005;91:358–66.
[10] Kojima Y, Usuki A, Kawasumi M, Kojima Y, Fukushima Y, Okada A, et al. Mechanical properties of nylon 6 – clay hybrid. J Mater Res 1993;8:1185–9.
[11] Supova M, Martynkova GS, Barabaszova K. Effect of nanofillers dispersion in polymer matrices: a review. Sci Adv Mater 2011;3:1–25.
[12] Hotta S, Paul DR. Nanocomposites formed from linear low density polyethylene and organoclays. Polymer 2004;45:7639–54.
[13] Durmus A, Woo M, Kasgoz A, Macosko CW, Tsapatsis M. Intercalated linear low density polyethylene (LLDPE)/clay nanocomposites prepared with oxidized polyethylene as a new type compatibilizer: structural, mechanical and barrier properties. Eur Polym J 2007;43:3737–49.
[14] Bureau MN, Perrin-Sarazin F, Ton-That MT. Polyolefin nanocomposites: essential work of fracture analysis. Polym Engng Sci 2004;44:1142–51.
[15] Lew CY, Murphy WR, McNally GM. Preparation and properties of polyolefin–clay nanocomposites. Polym Engng Sci 2004;44.
[16] Chaichana E, Jongsomjit B, Praserthdam P. Effect of nano-SiO_2 particle size on the formation of LLDPE/SiO_2 nanocomposite synthesized via the in situ polymerization with metallocene catalyst. Chem Engng Sci 2007;62:899–905.
[17] Jongsomjit B, Panpranot J, Praserthdam P. Effect of nanoscale SiO_2 and ZrO_2 as the fillers on the microstructure of LLDPE nanocomposites synthesized via in situ polymerization with zirconocene. Mater Lett 2007;61:1376–9.
[18] Wang Z, Li G, Xie G, Zhang Z. Dispersion behavior of TiO_2 nanoparticles in LLDPE/LLDPE/TiO_2 nanocomposites. Macromol Chem Phys 2005;206:258–62.
[19] Bureau MN, Ton-That MT, Perrin-Sarazin F. Essential work of fracture and failure mechanisms of polypropylene–clay nanocomposites. Engng Fract Mech 2006;73:2360–74.
[20] Dányádi L, Móczó J, Pukánszky B. Effect of various surface modifications of wood flour on the properties of PP/wood composites. Compos Part A 2010;41:199–206.
[21] Naveau E, Dominkovics Z, Detrembleur C, Jérôme C, Hári J, Renner K, et al. Effect of clay modification on the structure and mechanical properties of polyamide-6 nanocomposites. Eur Polym J 2011;47:5–15.
[22] Adhikari AR, Partida E, Petty TW, Jones R, Lozano K, Guerrero C. Fracture toughness of vapor grown carbon nanofiber-reinforced polyethylene composites. J Nanomater 2009:1–6.
[23] Musto P, Ragosta G, Scarinzi G, Mascia L. Toughness enhancement of polyimides by in situ generation of silica particles. Polymer 2004;45:4265–74.
[24] Bao SP, Tjong SC. Impact essential work of fracture of polypropylene/montmorillonite nanocomposites toughened with SEBS-g-MA elastomer. Compos Part A 2007;38:378–87.
[25] Dorigato A, Pegoretti A. Tensile creep behaviour of poly(methylpentene)-silica nanocomposites. Polym Int 2010;59:719–24.
[26] Dorigato A, Pegoretti A, Kolarik J. Nonlinear tensile creep of linear low density polyethylene/fumed silica nanocomposites: time-strain superposition and creep prediction. Polym Compos 2010;31:1947–55.
[27] Dorigato A, Pegoretti A, Migliaresi C. Physical properties of polyhedral oligomeric silsesquioxanes–cycloolefin copolymer nanocomposites. J Appl Polym Sci 2009;114:2270–9.
[28] Dorigato A, Pegoretti A, Penati A. Linear low-density polyethylene/silica micro- and nano-composites: dynamic rheological measurements and modelling. Express Polym Lett 2010;4:115–29.
[29] Prashantha K, Schmitt H, Lacrampe MF, Krawczak P. Mechanical behaviour and essential work of fracture of halloysite nanotubes filled polyamide 6 nanocomposites. Compos Sci Technol; in press.
[30] Williams JG, Rink M. The standardisation of the EWF test. Engng Fract Mech 2007;74:1009–17.
[31] Bárány T, Czigány T, Karger-Kocsis J. Application of the essential work of fracture (EWF) concept for polymers, related blends and composites: a review. Prog Polym Sci 2010;35:1257–87.
[32] Zhang H, Zhang Z, Yang JL, Friedrich K. Temperature dependence of crack initiation fracture toughness of various nanoparticles filled polyamide 66. Polymer 2006;47:679–89.
[33] Barany T, Foldes E, Czigany T, Karger-Kocsis J. Effect of UV aging on the tensile and fracture mechanical response of syndiotactic polypropylenes of various crystallinity. J Appl Polym Sci 2004;91:3462–9.
[34] Karger-Kocsis J. Towards phase transformation toughened semicrystalline polymers. Polym Bull 1996;37:119–24.
[35] Benavente R, Perez E, Qujada R. Effect of the comonomer content on the mechanical parameters and microhardness values in poly(ethylene-co-1-octadecene) synthesized by a metallocene catalyst. J Polym Sci, Part B: Polym Phys 2001;39:277–85.
[36] Demjen Z, Pukanszky B, Nagy J. Evaluation of interfacial interaction in polypropylene/surface treated $CaCO_3$ composites. Compos Part A 1998;29A:323–9.
[37] Pukanszky B. Particulate filled polypropylene: structure and properties. In: Karger-Kocsis J, editor. Polypropylene: structure blends and composites. London: Chapman and Hall; 1995. p. 1–70.

[38] Karger-Kocsis J, Benevolenski OI, Moskala EJ. Toward understanding the stress oscillation phenomenon in polymers due to tensile impact loading. J Mater Sci 2001;36:3365–71.
[39] Karger-Kocsis J, Czigany T, Moskala J. Stress oscillation in amorphous copolyesters due to tensile impact. Polym Engng Sci 1999;39:1404–11.
[40] Zhang L, Luo M, Sun S, Ma J, Li C. Effect of surface structure of nano-$CaCO_3$ particles on mechanical and rheological properties of PVC composites. J Macromol Sci, Phys 2010;49:970–82.
[41] Dorigato A, D'Amato M, Pegoretti A. Thermo-mechanical properties of high density polyethylene – fumed silica nanocomposites: effect of filler surface area and treatment. J Polym Res; in press.
[42] Lazzeri A, Zebarjad SM, Pracella M, Cavalier K, Rosa R. Filler toughening of plastics. Part 1—the effect of surface interactions on physico-mechanical properties and rheological behaviour of ultrafine $CaCO_3$/HDPE nanocomposites. Polymer 2005;46:827–44.
[43] Sudar A, Moczo J, Voros G, Pukanszky B. The mechanism and kinetics of void formation and growth in particulate filled PE composites. Express Polym Lett 2007;1:763–72.
[44] Gaucher-Miri V, Depecker C, Seguela R. Reversible strain-induced order in the amorphous phase of a low-density ethylene/butene copolymer. J Polym Sci, Part B: Polym Phys 1997;35:2151–9.
[45] Scardi P, Leoni M. Diffraction line profiles from polydisperse crystalline systems. Acta Crystall 2001;A57:604–13.
[46] Scardi P, Leoni M. Whole powder pattern modeling. Acta Crystall 2002;A58:190–200.
[47] Dorigato A, Pegoretti A, Frache A. Thermal stability of high density polyethylene – fumed silica nanocomposites. J Thermal Anal; submitted for publication.
[48] Jeol S, Fenouillot F, Rousseau A, Masenelli-Varlot K, Gauthier C, Briois J. Drastic modification of the dispersion state of submicron silica during biaxial deformation of poly(ethylene terephthalate). Macromolecules 2007;40:3229–37.